Unfolded Protein and Peptide Dynamics Investigated with Single-Molecule FRET and Correlation Spectroscopy from Picoseconds to Seconds†

Daniel Nettels, Armin Hoffmann, and Benjamin Schuler*

Biochemisches Institut, Universität Zürich, Winterthurerstrasse 190, 8057 Zürich, Switzerland

Received: August 30, 2007; In Final Form: February 8, 2008

Single-molecule fluorescence spectroscopy and correlation methods are finding increasing applications in the investigation of biomolecular dynamics, especially together with Förster resonance energy transfer (FRET). Here, we use the combination of start−stop experiments and classical fluorescence correlation spectroscopy (FCS) to obtain complete intensity auto- and cross-correlation functions from picoseconds to seconds for investigating the dynamics of unfolded proteins and peptides. In combination with distance information from single-molecule transfer efficiency histograms, we can analyze the data in terms of a diffusive process on a potential of mean force to obtain intramolecular diffusion coefficients. This allows us to extend our previous analysis of the time scales of chain dynamics into the low nanosecond range for peptides and into the microsecond range for a small cold shock protein (Csp). Dynamics in short unstructured peptides can be detected down to a time scale of about 10 ns, placing a lower limit on the time scales accessible with correlation methods and currently used dye pairs. We find no evidence for microsecond fluctuations in unfolded Csp, suggesting that its global chain dynamics occur predominantly in the tens of nanosecond range. We further investigate the position dependence of these dynamics by placing donor and acceptor dyes at different positions within the chain and find a decrease in the intramolecular diffusion coefficient by a factor of 3 upon moving one of the dyes toward the center of the polypeptide. Obtaining dynamic information on a wide range of time scales from single-molecule photon statistics will be of increasing importance for the study of unfolded proteins and for biomolecules in general.

Introduction

Elucidating the structure and dynamics of proteins in their denatured states, the starting point for the folding reaction, is a key prerequisite for a mechanistic understanding of protein folding. Correspondingly, there have been increasing recent efforts to address this question. Considerable information about the overall dimensions and residual structure of unfolded proteins has been obtained, especially from methods such as small-angle X-ray scattering[1,2] and NMR,[3−6] and a large number of studies have investigated the dynamics of unstructured peptides as models for segments of unfolded proteins.[7−10] A limitation of these methods is the averaging over a large ensemble of molecules, which complicates the analysis of distances and dynamics in heterogeneous systems, such as proteins under conditions where both unfolded and folded molecules are populated at the same time. Recently, single-molecule spectroscopy has emerged as a complementary method[11−15] that allows the separation of subpopulations in heterogeneous mixtures. In combination with Förster resonance energy transfer (FRET), it enables the measurement of intramolecular distances,[16,17] distance distributions,[17−19] and conformational dynamics down to the nanosecond time scale,[19,20] even for individual subpopulations of molecules.[21] The absence of averaging over many molecules allows spontaneous intramolecular distance fluctuations to be observed at equilibrium, without the need for perturbations to synchronize the ensemble. For this approach, the protein or peptide is labeled with fluorescent donor and acceptor dyes via amino groups or cysteine residues at specific positions of the chain. In the simplest type of experiment, freely diffusing molecules are observed during their transit through a confocal observation volume, where the donor chromophore is excited by the laser beam. Depending on the distance r to the acceptor, energy transfer results, with a rate that determines the relative probabilities of photon emission from donor and acceptor. Correspondingly, both distances and distance dynamics within the protein can be measured from the detected donor and acceptor photons via the transfer efficiency and its fluctuations. The Förster radii of currently available dye pairs suitable for single-molecule experiments in the range of about 5 nm allow measurements on relatively large distances, making this approach highly complementary to NMR, from which, typically, distance information and dynamics on shorter length scales have become available.

Here, we extend our analysis of conformational dynamics from single-molecule FRET experiments to the entire range of time scales available from confocal experiments on freely diffusing molecules. By combining conventional fluorescence correlation spectroscopy (FCS) with start−stop experiments, we obtain correlation data from picoseconds to seconds. We use this approach to identify the time scales on which conformational dynamics occur in the unfolded state of the cold shock protein (Csp) from *Thermotoga maritima*, a small (7.5 kDa) β-barrel protein that exhibits two-state thermodynamics and kinetics,[22−26] and to investigate the dependence of chain dynamics on the position of the chromophores within the polypeptide. Moreover, we test the limits of the method for detecting dynamics in the

† Part of the "Attila Szabo Festschrift".

* To whom correspondence should be addressed. E-mail: schuler@bioc.uzh.ch.

10.1021/jp076971j CCC: $40.75
Published on Web 04/15/2008

short distance regime with unstructured and stiff peptides and compare them to calculated correlation functions using a model that describes the distance dynamics as a diffusive process on a free-energy surface.

Materials and Methods

Samples. Labeled Csp and polyproline peptides were prepared as described previously.[17,18,24] The unstructured peptide with sequence $G(AGQ)_6AGC$ was purchased from GL Biochem (Shanghai, China) and labeled analogous to the polyproline peptides by reacting it sequentially via its amino and sulfhydryl groups, respectively, with Alexa 488 succinimidyl ester and Alexa 594 maleimide (Molecular Probes/Invitrogen, Eugene, Oregon), followed by size-exclusion chromatography (Superdex Peptide HR 10/30, Amersham GE Biosciences, Piscataway, NJ) to separate the product from unreacted dye. All measurements were performed in 50 mM sodium phosphate buffer adjusted to pH 7, containing 0.001% Tween 20 to prevent surface adhesion of the polypeptides. High-purity GdmCl solutions (Pierce, Rockford, IL) were used for denaturation experiments. Transfer efficiency histograms were recorded at peptide concentrations of 50 pM. Correlation experiments were performed at a 500 pM protein/peptide concentration to optimize signal contrast.

Single-Molecule Instrumentation. Single-molecule fluorescence was observed using a PicoQuant MicroTime 200 confocal microscope equipped with a cw solid-state diode-pumped laser (Coherent Sapphire 488-200) operating at 488 nm (average radiant power at the sample: 150μW), a 1.2 NA, 60× microscope objective (Olympus UplanApo 60×/1.20W), and a 100 μm confocal pinhole. A dichroic mirror (Chroma 585DCXR) separated donor and acceptor fluorescence. For donor−acceptor cross-correlation measurements, the donor and acceptor fluorescence is detected by a pair of two avalanche photodiodes (APDs, Perkin-Elmer Optoelectronics SPCM-AQR-15). For autocorrelation measurements, each fluorescence component was divided further randomly by a 50/50 beam splitter between a pair of APDs. In both configurations, additional interference filters (Chroma HQ525/50 and Omega 525AF45 for the donor APDs, Chroma 600HQLP and HQ640/100 for the acceptor APDs) completed spectral separation of the sample fluorescence and served to suppress the mutual detection of APD breakdown flashes in the infrared.[27] Each of the two APD pairs was connected to a photon counter (two PicoHarp 300, PicoQuant). In their histogram mode, which we used for the measurements at 500 pM Csp, the two input channels of these counters operate as start and stop channels. The measured time intervals between start and stop were histogrammed in 256 ps bins. To avoid cross-talk between the two channels at short time intervals and to simplify data analysis (see below), an electronic time delay $t_0 \approx 500$ ns was imposed onto the stop channel. For conventional FCS measurements, the photon events on the four detectors were recorded by a TimeHarp 200 or a PicoHarp 300 counting card (PicoQuant) equipped with a four channel router. FCS diagrams were recorded by the data acquisition software SymphoTime (PicoQuant) with 2−30 min of integration time.

Processing of the Start−Stop Raw Data. The histograms recorded in start−stop measurements represent unnormalized interphoton time distributions $\tilde{\phi}_{ij}(t)$ (i,j = A,D), which, in the limit of low mean photon rates, can be related to the fluorescence correlation function $g_{ij}(\tau)$ by[21]

$$\tilde{\phi}_{ij}(t) = Ae^{-t/\tau_{ij}} g_{ij}(t - t_0) \qquad (1)$$

This approximation is valid as long as $t \ll \tau_{ij}$, where τ_{ij} denotes the mean interphoton time. When the correlation function $g_{ij}(\tau)$ is symmetric with respect to $\tau = 0$, τ_{ij} can be obtained from the measured histogram (interpolated by the function $\phi_m(t)$) by numerically minimizing the integral

$$\int_0^{t_0} (\phi_m(t)e^{t/\tau_{ij}} - \phi_m(2t_0 - t)e^{(2t_0 - t)/\tau_{ij}})^2 dt$$

Here, the delay t_0 is, to a first approximation, taken from the histogram bin with the minimum number of counts. The resulting τ_{ij} are typically in a range of 10−20 μs, in good agreement with the mean interphoton time during the passage of a labeled polypeptide through the confocal volume. Multiplication of the raw data by $e^{t/\tau_{ij}}$ then yields the correlation function, except for a scaling factor A that is obtained from a combined global fit to the start−stop data and the FCS data as described in the following section. The cross-correlation $g_{AD}(\tau)$ is, in general, not perfectly symmetric with respect to $\tau = 0$ (see refs 28 and 29). The procedure described above can nevertheless be applied since the asymmetry arising in the systems studied here occurs mainly on the time scales of singlet-state photophysics, that is, in the nanosecond range.

Global Analysis of Start−Stop Data and FCS Data. The start−stop data (corrected according to eq 1) and the FCS data represent the fluorescence correlation functions on different time scales and have only a small overlap in the microsecond range. For combining and interpreting the two data sets, we globally fit them with a model function, $g_{ij}(t - t_0^{(ij)})$, (i,j = A,D), where, in the case of the start−stop data, the function has an additional amplitude A_{ij} as a prefactor. The $g_{ij}(\tau)$ is of the form

$$g_{ij}(\tau) = 1 + \frac{(1 - c_{ab}^{(ij)}e^{-|\tau|/\tau_{ab(ij)}})(1 + c_{cd}^{(ij)}e^{-|\tau|/\tau_{cd}})(1 + c_T^{(ij)}e^{-|\tau|/\tau_{T(ij)}})}{n_{ij}\left(1 + \frac{|\tau|}{\tau_D}\right)\left(1 + \frac{|\tau|}{s^2\tau_D}\right)^{1/2}} \qquad (2)$$

where the three terms in the numerator describe photon antibunching (ab), conformational peptide dynamics (cd), and triplet blinking (T). The denominator describes the effect of diffusion of the peptides through the confocal volume,[30] which is assumed to be of Gaussian shape with a ratio of axial over lateral radii of $s = \omega_2/\omega_1$; n_{ij} is the average effective number of peptides in the confocal volume contributing to $g_{ij}(\tau)$, and τ_D is given by $\tau_D = \omega_1^2/4D_t$, where D_t is the translational diffusion coefficient. All parameters in eq 2 lacking the indices ij are assumed to be the same in $g_{DD}(\tau)$, $g_{AA}(\tau)$, and $g_{AD}(\tau)$. These parameters are the common fit parameters of the global analysis of the 3 × 2 data sets presented in Figure 1. For the autocorrelations $g_{ii}(\tau)$, the amplitudes $c_{ab}^{(ii)}$ are set to unity ($c_{ab}^{(ii)} = 1$), that is, the autocorrelation is $g_{ii}(\tau=0) = 1$ at time zero, as two coincidently emitted photons must originate from two different fluorophores and are hence uncorrelated. The amplitudes $c_{cd}^{(ij)}$, associated with conformational dynamics, are positive (correlated) in the case of the autocorrelation functions and negative (anticorrelated) in the case of the cross-correlation functions. For the fitting of the cross-correlation in Figure 1, we set $c_T^{(AD)}$ in eq 2 equal to zero since the fluorescence cross-correlation is (to good approximation) not influenced by triplet blinking at low excitation rates (see Results section). Further, we note that, as indicated in the last section, the cross-correlation $g_{AD}(\tau)$ is asymmetric with respect to $\tau = 0$ on the nanosecond time scale relevant for photophysical processes.[28,29,31−33] This

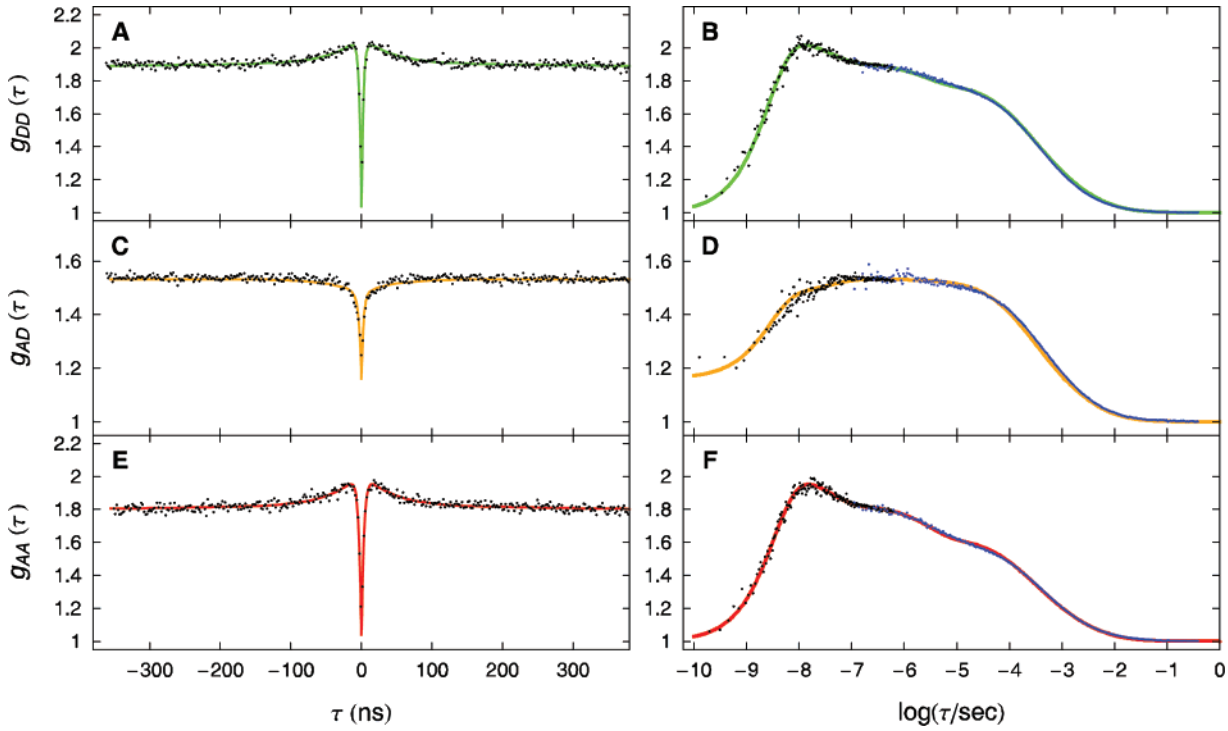

Figure 1. Measured intensity correlation functions for unfolded Csp in 4 M GdmCl. The left panels (A,C,E) show the results from start−stop experiments (black data points), the right panels (B,D,F) the complete correlation functions from picoseconds to 1 s, obtained by combining the start−stop experiments with conventional FCS measurements (blue data points). The result of the global fit is shown as a solid line in green for the donor intensity autocorrelation (A,B), in red for the acceptor intensity autocorrelation (E,F), and in yellow for the cross-correlation (C,D).

asymmetry can be approximated by setting $\tau_{ab}^{AD} = \tau_{ab}^{DD}$ for $\tau > 0$ and $\tau_{ab}^{AD} = \tau_{ab}^{AA}$ for $\tau < 0$, as we did in the fit of $g_{AD}(\tau)$ in Figure 1. Deviations from this approximation may contribute to the slight imperfections in the fit of the cross-correlation functions (Figure 1c,d).

Time-Resolved Anisotropy. Anisotropy decay data were recorded with a custom-built fluorescence lifetime spectrometer. The samples were 1 μM donor-only-labeled Csp under native and unfolding conditions (4 M GdmCl), both with 50 mM sodium phosphate buffer adjusted to pH 7.0 and 0.001% Tween 20. The fluorophores were excited at 470 nm by vertically polarized laser pulses from a LDH 470 diode laser (PicoQuant). A high degree of linear polarization was achieved by using a Glan-Thompson polarizer (extinction ratio > 100 000:1). The laser beam diameter was confined by a 1 mm circular aperture centered at the laser entrance opening of the cuvette holder (TLC 50F, Quantum NorthWest). A narrow cone of fluorescence light, emitted in the perpendicular direction with respect to the laser beam, was collimated by a planoconvex lens ($f = 40$ mm). The opening angle of the cone was defined by a circular 2 mm aperture positioned at a distance of 16 mm from the center of the cuvette. The collimated light passed an analyzing polarizer (of Glan-Thompson type) and a band-pass filter (Chroma, z 582/15) before it was focused onto a microchannel plate PMT (R3809U-50, Hamamatsu). The output pulses of the PMT were preamplified (by a PAM 102-M, PicoQuant) and recorded by a photon counting module (PicoHarp 300, PicoQuant), which measures the times between laser pulses (as provided from the synchronization signal of the laser driver) and the fluorescence photon arrival times at the PMT, from which fluorescence decay histograms with 8 ps bin width were formed. The overall instrument response function (IRF) of the system was measured to have a fwhm of $\Delta_{IRF} = 80$ ps. The repetition period of the laser pulses was 50 ns, whereas the fluorescence lifetime of the donor dye was about 4 ns. Overlap between adjacent excitation−emission cycles is hence negligible.

Two fluorescence decays, $I_V(t)$ and $I_H(t)$, were measured for each sample with the analyzing polarizer in the vertical and in horizontal orientation, respectively. From these decays, the anisotropy as a function of time was determined as[34,35]

$$r(t) = \frac{I_V(t) - GI_H(t)}{I_V(t) + 2GI_H(t)} \tag{3}$$

where G is a correction factor compensating for the slightly different instrumental detection sensitivity for vertically and horizontally polarized photons. We measured $G = 1.02$ for our instrument following standard procedures.[34,35] To the resulting anisotropy decay data, we fit the function[36]

$$r(t) = ((r_0 - r_\infty)e^{-(t-t_0)/\tau_{eff}} + r_\infty)e^{-(t-t_0)/\tau_M} \tag{4}$$

which models the decay as the combined effect of restricted dye rotation near the protein surface (decay constant τ_{eff}) and the rotational motion of the entire molecule, that is, the protein−dye complex (decay constant τ_M). t_0 is the time delay between the registration of the sync signal of the laser driver and the actual fluorophore excitation at the sample site, and r_0 is the fundamental anisotropy of the dye molecule. We measured $r_0 = 0.38$ for Alexa 488 in a matrix of 99% glycerol at −10 °C, where rotational motion is negligible. r_∞ in eq 4 is the residual anisotropy measured at long times in the absence of rotation of the protein carrying the dye. For the fit, we considered only data with times t that approximately satisfy $t > t_0 + 2\Delta_{IRF}$ and used t_0, r_∞, τ_{eff}, and τ_M as fit parameters. Using this procedure, we avoid the error-prone deconvolution of the fluorescence decays, $I_V(t)$ and $I_H(t)$, before calculating eq 3.

Results

Analysis of Fluctuations from Picoseconds to Seconds. Distance dynamics within a FRET-labeled protein lead to fluctuations of the transfer rate between the dyes, and thus of the instantaneous photon emission rates of the donor and acceptor, on the time scale of the dynamics. Consequently, chain dynamics can be obtained from the corresponding photon statistics using correlation methods.[30] In practice, classical FCS is typically limited to time scales above about 1 μs because of the dead time of detectors and counting electronics in the >100 ns range. Shorter times become accessible with experiments where two separate detectors are used to record consecutive photons.[28,31,37−43] From such Hanbury Brown and Twiss experiments, interphoton times can be determined with a time resolution limited only by the timing accuracy of the counting electronics (several picoseconds for latest-generation time-correlated single-photon counting (TCSPC) cards[44,45]) and the jitter of the detectors (several hundred picoseconds for the Perkin-Elmer SPCM-AQR avalanche photodiodes[44] typically used in single-molecule experiments). The resulting interphoton time distributions can be related directly to the intensity correlation function.[21,39,46] The combination of these two methods thus enables access to time scales from picoseconds up to the order of the length of the observation time.[44,45] In practice, the photon antibunching signature in the correlation function[38,47] on the time scale of the fluorescence lifetime of the chromophores (typically a few nanoseconds) constitutes the lower end of the time window usable for extracting distance dynamics. (Dynamics on the time scale of the fluorescence lifetime of the dyes can be investigated by analyzing fluorescence lifetime decays with a model including diffusive distance dynamics.[19,48,49]) The upper limit of the exploitable time range is about 1 ms, the maximum observation time for protein molecules freely diffusing through a diffraction-limited confocal volume. (Longer times can be accessed by slowing down diffusion or by observation of immobilized molecules.)

A complete and robust way of analyzing such correlation data is to combine the results from start−stop experiments and FCS and to utilize both donor and acceptor autocorrelation and acceptor−donor cross-correlation measurements. The resulting three complete correlation functions ranging from picoseconds to seconds can then be interpreted in terms of a global fit with a model including all relevant processes[50] (Figure 1). The processes almost universally observed are singlet-state photophysics, resulting in pronounced photon antibunching in the range of a few nanoseconds, triplet-state photophysics in the microsecond range, and fluctuations originating from the diffusion of molecules through the focus in the millisecond range. Rotational dynamics can also contribute to the correlation functions,[38,47] but for the cases investigated here, the free rotation of the chromophores dominates, with rotational correlation times of a few hundred picoseconds (Figure 2). Especially important for our application of the method here is that in the presence of intramolecular distance fluctuations, an additional component is expected in the correlation functions of a FRET-labeled sample, which has been used to measure long-range dynamics in unfolded proteins.[21] Figure 1 shows the three complete correlation functions for terminally labeled Csp unfolded in 4 M guanidinium chloride (GdmCl), fit globally with eq 2, which takes into account all of these components (see Materials and Methods). Rapid conformational dynamics of the unfolded chain[21] result in a positive amplitude component in the autocorrelations and a negative amplitude component in the cross-correlation with $\tau_{cd} = 40$ ns. The dynamics of all processes that can be detected in our system with single-molecule FRET are thus captured in the entire range of accessible times from picoseconds to milliseconds.

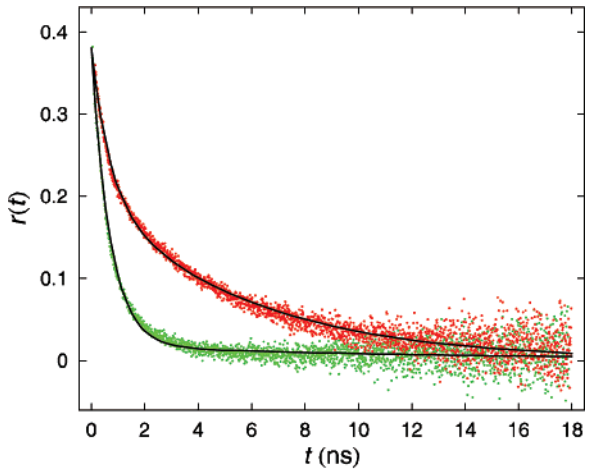

Figure 2. Time-resolved fluorescence anisotropy decay $r(t)$ of folded (red) and unfolded (green) Csp labeled only with a donor dye. While the fluorescence emission for folded Csp indicates significant residual anisotropy ($r_\infty = 0.20$, $\tau_M = 5.7$ ns), the anisotropy of Csp unfolded in 4 M GdmCl can be well approximated by a single exponential decay with a time constant of 0.74 ns, indicating rapid reorientation of the fluorophore. Fits to eq 4 are shown as black lines.

Time Scales of Unfolded State Dynamics in Csp. In the analysis of start−stop experiments, we have identified fast Brownian dynamics of the polypeptide chain ends relative to each other in terminally labeled unfolded Csp on the time scale of ~50 ns (see ref 21). The time scale of these dynamics is of fundamental interest to a quantitative understanding of the folding process because it is closely related to the effective diffusion coefficient underlying a description of protein folding as a diffusive process on a free-energy surface, which is frequently used in statistical mechanical models.[51,52] The determination of such elementary time scales has gained even more relevance in view of the discovery of proteins folding in microseconds[53] and faster,[54] close to the expected "speed limit"[7,53,55,56] of folding. A comparison with the time scales of chain dynamics found in unstructured model peptides[7−9,49,57] and the observation of dynamics on a similar time scale for a series of other unfolded proteins (Nettels, Hillger, Wuttke, and Schuler, unpublished observations) suggest that long-range chain dynamics in the nanosecond range are a universal feature of unfolded proteins. The question remains, however, whether dynamics on longer time scales also contribute, especially in view of the microsecond phases frequently observed in protein folding kinetics.[58,59]

The availability of the complete correlation functions now allows us to address this question for Csp (Figure 1). Of particular value for analyzing distance dynamics is the fact that even though the component corresponding to distance dynamics must show up in all three correlation functions, it results in an amplitude of opposite sign for auto- and cross-correlations.[29,60] This difference allows us to distinguish distance dynamics from other processes, most importantly triplet blinking, which typically occurs in the microsecond range.[61] Figure 1 shows this characteristic signature for chain dynamics with a relaxation time of 40 ns; both donor (Figure 1a,b) and acceptor (Figure 1e,f) autocorrelations exhibit a component with positive amplitude, while the cross-correlation (Figure 1c,d) contains a component with negative amplitude that can be described with the same time constant. In contrast, however, the autocorrela-

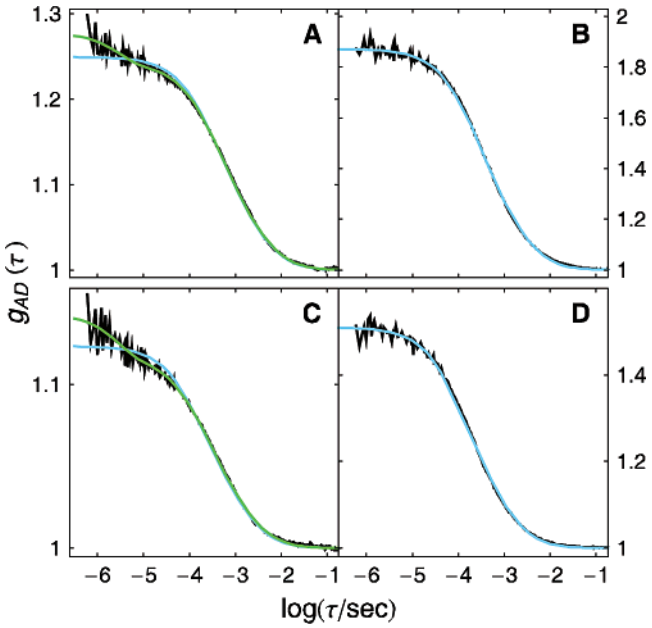

Figure 3. Cross-correlation functions for unfolded Csp (A,B) and for Pro20 (C,D) at different excitation rates. Whereas a residual triplet component is clearly visible at high laser power (A,C, 350 μW), it is absent at low power (B,D, 8 μW). Fits including only translational diffusion are shown in blue, and fits including an additional triplet component are shown in green.

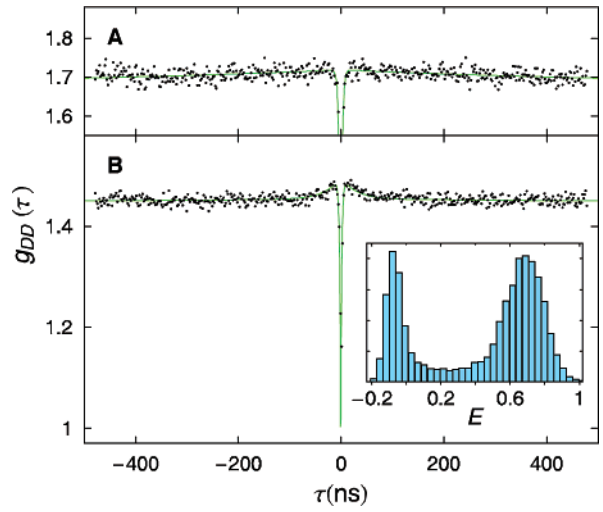

Figure 4. Donor intensity autocorrelation functions measured for Pro20 (A) and the labeled unstructured peptide G(AGQ)$_6$AGC in 8 M GdmCl (B). The unstructured peptide shows rapid end-to-end distance dynamics with a characteristic time of τ_{cd} = 15 ns; the dynamics in Pro20 are too rapid to be detected, as expected from simulations. The inset in (B) shows the transfer efficiency histogram of G(AGQ)$_6$AGC with $\langle E \rangle$ = 0.69 used for calculating the mean-squared end-to-end distance. The peak at $E \approx 0$ is due to molecules with an inactive acceptor.[17]

tions exhibit a large change in amplitude in the microsecond range (Figure 1b,f), but not the cross-correlation (Figure 1d). This is the typical signature found for triplet dynamics,[50,60] and already indicates the absence of a strong contribution of distance fluctuations on that time scale. However, a slight influence of triplet dynamics on the cross-correlation cannot be excluded, first because of the slight overlap of the donor emission spectrum with the wavelength range for acceptor detection (effectively resulting in a small contribution of the donor autocorrelation to the observed cross-correlation) and second because the effect

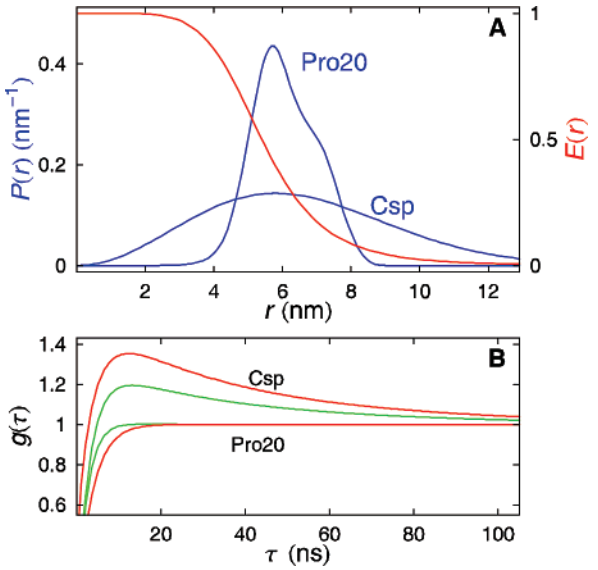

Figure 5. (A) End-to-end distance probability density function $P(r)$ and (B) the resulting calculated acceptor (red) and donor (green) intensity autocorrelation functions for Csp and Pro20. $P(r)$ for Csp is derived from experimental data[18] and $P(r)$ for Pro20 from simulations.[62] The distance dependence of the transfer efficiency E is shown in (A).

of populating the triplet state in one dye on the emission of the other dye is currently unknown for the chromophores used here. In general, however, triplet states are increasingly populated at high excitation rates.[61] To further investigate the presence of a microsecond component originating from distance fluctuations, and in particular the possibility of accidental cancellation of triplet and distance dynamics in the cross-correlation function, we thus performed FCS measurements at different excitation rates and compared them to measurements on Pro20, for which microsecond distance fluctuations are not expected (Figure 3; note that start−stop experiments are not feasible at low excitation rates because of the resulting low count rates). While at high laser power (350 μW) a residual triplet component is visible, at the lowest laser power (8 μW), the cross-correlations both for unfolded Csp and Pro20 show no evidence for a change in the correlation amplitude in the microsecond range (and clearly no component with negative amplitude, as would be expected in the case of distance dynamics) and are well fit by a correlation function taking into account only translational diffusion. Within the accuracy of the method, we thus find no evidence for microsecond distance fluctuations in Csp at 4 M GdmCl, suggesting that the dynamics in the unfolded state of this two-state protein are dominated by diffusive chain reconfiguration in the tens of nanosecond range.

Exploring the Limits of the Method in the Nanosecond Range. To further investigate the sensitivity of the method in the nanosecond range, we present two examples of measurements on peptides with previously characterized dynamic properties. The first example (Figure 4a) is a polyproline peptide (20 residues, Pro$_{20}$), which we used earlier as a reference for a polypeptide with negligible intramolecular distance dynamics above the nanosecond range.[21,24] Molecular dynamics simulations have shown significant flexibility of polyproline peptides,[17,62] and very recent simulations including the fluorophores[62] give an even more detailed picture of the dynamics involved. Despite the significant width of the distance distribution (Figure 5), the dynamics of the system remain undetected in start−stop experiments (Figure 4a) because their characteristic time scale is too close to the fluorescence lifetime of the

fluorophores (~2−4 ns) and thus coincides with the photon antibunching phase in the correlation function (Figure 5b). This observation is in agreement with molecular dynamics simulations, which place the end-to-end dynamics of the peptide in the 2 ns range.[17,62] A better characterization of all fast photophysical processes involved might allow the deconvolution of dynamic information even in this time range, but our lack of quantitative understanding of processes such as singlet−singlet annihilation for the chromophores currently prevents a more complete analysis. However, polyproline peptides remain a valuable reference for correlation experiments because of their large stiffness and their lack of dynamics on longer time scales than a few nanoseconds.

The second example is the unstructured peptide $(G(AGQ)_6AGC)$ of the kind previously investigated in much detail in experiments employing the contact quenching of tryptophan triplet states by cysteine[8,57,63] to quantify the kinetics of elementary loop formation in polypeptides. While we were not able to detect chain dynamics for this peptide in the absence of denaturants (because of the narrow distance distribution with a small mean distance located in the plateau region of the Förster curve), we were able to observe peptide dynamics in the presence of 8 M GdmCl, where the chain is sufficiently expanded (Figure 4b). To obtain an effective end-to-end diffusion coefficient, we describe the relative motion of the chain ends as a diffusive process on the potential of mean force that corresponds to the end-to-end distance distribution of the labeled peptide. By combining these conformational dynamics with the distance-dependent stochastic photon emission from the coupled dye pair, the complete photon statistics of the system can be obtained.[29] We use a recently developed theory[46] that allows us to calculate the intensity correlation functions of donor and acceptor emission numerically.[21] Briefly, if we assume for the unfolded protein the end-to-end distance distribution of a Gaussian chain[8,57,63]

$$p_{eq}(r) = 4\pi r^2(2\pi\langle r^2\rangle/3)^{-3/2}\exp(-3r^2/2\langle r^2\rangle) \qquad (5)$$

protein dynamics can be combined with the photophysics of FRET in the rate matrix

$$\mathbf{K} = D\partial/\partial r\, p_{eq}(r)\, \partial/\partial r\, (p_{eq}(r))^{-1}\mathbf{I} + \mathbf{K}_0(r) \qquad (6)$$

where D is the relative diffusion coefficient of the chain ends, $\mathbf{K}_0(r)$ describes the distance-dependent kinetics of interconversion between the electronic states involved, and $\mathbf{I}$ is the 4×4 identity matrix. The time dependence of all electronic and conformational transitions in the system is then described by the rate equation $d\mathbf{p}/dt = \mathbf{Kp}$, where $\mathbf{p}$ is the vector of the populations of the electronic states. By discretizing the diffusion operator, the problem is reduced to matrix algebra, and the intensity correlation functions can be calculated to high accuracy with numerical methods.[21] All parameters needed to define the model in terms of our system are known; the photophysical rate constants of the FRET process were measured independently,[21] and $p_{eq}(r)$ is defined uniquely by the mean-squared end-to-end distance $\langle r^2\rangle$, which we calculate[18,21,24] from the corresponding mean transfer efficiency of $\langle E\rangle \approx 0.69$ (Figure 4b, inset) as 4.8 nm. We can thus determine the only remaining parameter, the effective end-to-end diffusion coefficient D, by adjusting it such that the calculated intensity correlation function fits the experimental result.

From the decay time of the intensity correlation function of 15 ns (Figure 4b), we obtain an intramolecular end-to-end diffusion coefficient of 0.27 nm^2/ns. Assuming that the diffusion coefficient is inversely proportional to the viscosity of the solvent,[49,57,64] we get a viscosity-corrected diffusion coefficient of 0.64 nm^2/ns. This result is close to the value of 0.53 nm^2/ns for Csp in 8 M GdmCl,[21] suggesting that the chains' dynamics are very similar at these high concentrations of denaturant. The value found here is somewhat larger than the diffusion coefficients determined from viscosity-dependent tryptophan triplet quenching experiments for the same AGQ-repeat sequence[57,63] (between 0.08 and 0.17 nm^2/ns). Even though a direct comparison is difficult because those measurements were not performed at 8 M GdmCl, part of the difference could be caused by relatively small deviations from the distance distributions assumed in the analysis and the fact that the two methods probe different parts of the equilibrium distribution.

Overall, our measurements on this short unstructured peptide show the accuracy of correlation methods down to ~10 ns. At shorter distances and smaller time scales, fluorophores with smaller Förster radii and shorter fluorescence lifetimes would become necessary to use this approach. On the time scale of a few nanoseconds, dynamic information is available from the analysis of fluorescence lifetime decays;[48,49] even faster dynamics require methods such as pump−probe laser spectroscopy or NMR.

Position Dependence of Intramolecular Dynamics. Previously, we have investigated the intramolecular dynamics of unfolded Csp for a variant with the fluorescent labels at the termini (residue 2 and 67) of the polypeptide chain.[21] Here, we extend our analysis to variants where one of the chromophores is located at the carboxy terminus (residue 67), the other at position 2, 10, 21, 22, or 34 (Figure 6a), to probe the dependence of intramolecular diffusion on the position within the chain. Start−stop and correlation experiments were performed and analyzed as described above for the unstructured peptide. The resulting fluorescence intensity correlation times τ_{cd} corresponding to chain dynamics in these variants are shown in Figure 6b as a function of the sequence separation of the labeled residues. We observe a steady increase of τ_{cd} upon moving the second fluorophore from the terminus toward the middle of the polypeptide chain, from 40 to 67 ns. This increase is reminiscent of recent triplet−triplet energy-transfer experiments on unstructured Gly-Ser peptides, where a continuous decrease of the contact rate was found with increasing length of the tail segment.[65]

An advantage of investigating intramolecular dynamics with FRET is that both the distance distributions[18] (via measurements of the transfer efficiency) and dynamic information (via correlation functions[21] or fluorescence lifetime decay analysis[48,49]) can be obtained. The use of single-molecule spectroscopy additionally allows the separation of subpopulations[18,21,24,43,66] necessary for performing such an analysis even under conditions where folded and unfolded molecules coexist. As explained above, the fluorescence intensity correlation time τ_{cd} in combination with the shape of the end-to-end distance distribution can be used to extract intramolecular diffusion coefficients. As for the unstructured peptide, we use the end-to-end distance distribution of a Gaussian chain, which has been shown to be a good approximation for unfolded Csp.[18] By adjusting the intramolecular diffusion coefficient D such that calculation and experiment agree, D can be determined. The chain reconfiguration time τ_r (the decay time of the end-to-end distance autocorrelation function) is then obtained from $\tau_r \simeq \langle r^2\rangle/6.2D$ (see ref 21).

Figure 6b also shows the root-mean-square distance (rms r) between the fluorophores in the unfolded Csp variants,[18] and Figure 6c shows the intramolecular diffusion coefficient as a

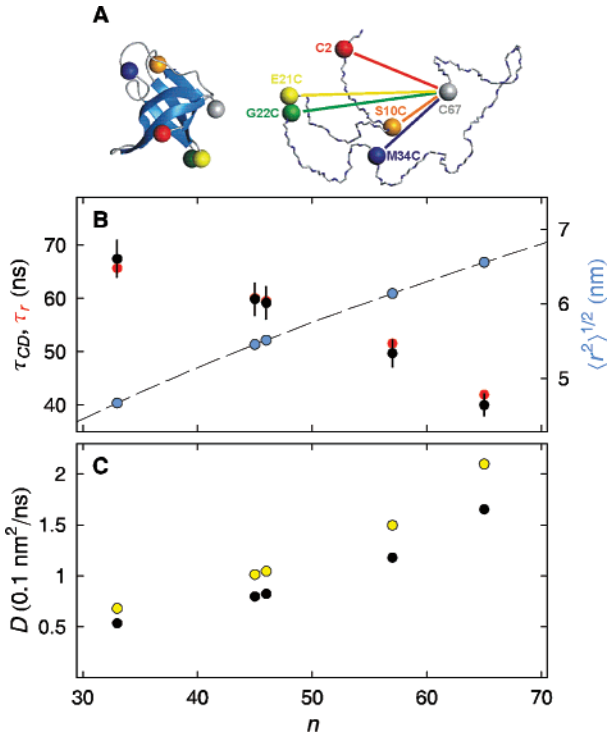

Figure 6. Position dependence of intramolecular dynamics in unfolded Csp (4 M GdmCl). (A) Schematic of folded (left) and unfolded (right) Csp with the sites for dye attachment for Förster resonance energy transfer indicated by colored spheres. For every variant, one dye was reacted with Cys at position 67 and the second dye with a Cys at one of the other positions shown. (B) Decay time τ_{cd} of the intensity correlation function, decay time τ_r of the intramolecular distance correlation function (the reconfiguration time), and root-mean-square distance $\langle r^2 \rangle^{1/2}$ between the probes as a function of their separation within the polypeptide chain n. The $\langle r^2 \rangle^{1/2}$ as a function of n was calculated from the apparent persistence length of 0.87 nm determined previously for unfolded Csp in 4 M GdmCl.[18] (C) Relative intramolecular diffusion coefficient D as a function of sequence separation calculated from the values in (B) both with (yellow) and without (black) viscosity correction, indicating slowed dynamics when one of the dyes is moved toward the middle of the chain. The error bars in (B) are our estimates of the experimental error.

function of sequence separation. As expected, the mean distance between the dyes decreases as they are moved closer together in sequence. For a diffusion coefficient independent of the probe position, smaller sequence separation would be expected to result in faster chain reconfiguration, and thus to a decrease in τ_{cd}, because of the smaller configuration space available. By contrast, upon moving one of the dyes toward the middle of the chain, we observe an increase in τ_{cd} from 40 to 67 ns, corresponding to a decrease in D by a factor of 3 (Figure 6c). This suggests that the faster relaxation expected from the narrowing of the distance distribution within the chain must be overcompensated by slower chain dynamics. Note that Figure 6c contains both the diffusion coefficients in 4 M GdmCl (black) and the viscosity-corrected values[49,57,64] (yellow) for direct comparison with experiments at other denaturant concentrations.

One expected contribution to this decrease in D is the increase in length of the chain segments that need to move in order to allow translational diffusion of one probed position with respect to the other. The relative intramolecular distance diffusion coefficient D can formally be regarded as the sum of two diffusion coefficients D_1 and D_2, which describe the relative diffusion of two positions in the chain, assuming that one or the other was fixed in space. If we further assume that $D_1 = D_2$ for the relative diffusion of the chain ends and that D_1 and D_2 were mutually independent, D could never decrease by more then a factor of 2, even if one residue was effectively immobilized. Our observation of a decrease of D by a factor of 3 suggests that D_1 and D_2 are not independent and that both the internal and the terminal residues are affected in their motion within the unfolded chain. One possibility is that the internal residue is effectively shielded by the tail segment, resulting in additional internal friction also for the terminal residue. Note, however, that the reconfiguration time, which is the parameter proportional to the preexponential factor in Kramers-like models of protein folding[52,67,68] and thus most relevant for the fast formation of contacts within an unfolded protein, varies by only about 50% for the different segments (Figure 6b). This suggests that the position dependence of chain reconfiguration has only a moderate effect on the overall time scales of protein folding, at least for all but the fastest folding proteins.

Discussion

Correlation methods are a versatile tool for analyzing dynamic processes and have recently gained increasing popularity especially in combination with fluorescence detection.[30] Depending on the experimental setup, processes from picoseconds to many hours are accessible, if the molecules are suitably immobilized. Here, we focus on measurements on freely diffusing molecules, a common approach that has the advantages that surface interactions that could interfere with the dynamics can largely be excluded and that reliable photon statistics become available simply by waiting for a sufficient number of molecules to cross the confocal volume. Of course, the accessible time scales are then limited by the diffusion time of a molecule through the confocal volume, but many biomolecular processes occur in the submillisecond range and can thus be studied relatively easily over several orders of magnitude in time.

Taking our previous observations of unfolded state dynamics[21] with a Hanbury Brown and Twiss-type instrument[43] in the tens of nanosecond range as a starting point, we are now extending the time scales used in our analysis to both shorter and longer times. To probe the accessibility of shorter times, we investigated two small peptides, a stiff polyproline peptide and an unstructured peptide with the properties of a random coil. While the polyproline dynamics expected on the ~2 ns time scale from simulations[17,62] remain undetected, the dynamics of the unstructured peptide can be detected, at least in high concentrations of GdmCl, with a correlation time of 15 ns and a resulting intramolecular diffusion coefficient that is in approximate agreement with tryptophan triplet quenching studies.[57,63] This time scale places an approximate lower bound on the dynamics accessible from correlation analyses with the Förster radii and fluorescence lifetimes of the typical dye pairs currently available for single-molecule FRET. On shorter time scales, the analysis of fluorescence lifetime decays[19,48,49] on the same type of samples can be used to extract information on dynamics down to times of about 50 ps. Time scales above the typical dead times of detectors and counting electronics are easily accessible with classical FCS measurements. By combining them with the start−stop experiments, fluctuations from picoseconds to milliseconds become available and can be analyzed with a global fit using a model that contains all dynamic processes in this time window. Here, we used this information to investigate the existence of slow unfolded state dynamics of the small two-state protein Csp.

The existence of submillisecond components in Csp folding dynamics has been difficult to clarify. Previous pressure-[70] and

temperature-jump[71] experiments both on closely related cold shock proteins and the FRET-labeled Csp used here (Kubelka, J.; Schuler, B.; Eaton, W. A. Unpublished observation) with a time resolution in the microsecond range and below have not lead to an identification of any kinetic components in the submillisecond range. However, such kinetic ensemble experiments require a change in volume or enthalpy connected to the conformational change involved to allow a perturbation of the system. By contrast, single-molecule experiments monitor spontaneous fluctuations at equilibrium and thus lack this requirement. This advantage has allowed us to identify the previously elusive unfolded state dynamics of Csp on the tens of nanosecond time scale.[21] With the extended time scale available through the combination of start−stop experiments with FCS, we were now able to extend our analysis into the microsecond range and find no indication for distance fluctuations in unfolded Csp on time scales above the tens of nanosecond range.

The absence of microsecond components in the unfolded state dynamics and the folding kinetics of Csp is indicative of a lack of specific interactions within the polypeptide before it crosses the main transition state for folding, in contrast to observations on a wide range of larger proteins or proteins with cofactors,[59] where microsecond phases are frequently observed. While the results presented here cannot exclude short-range interactions in specific segments of the polypeptide leading to slow low-amplitude dynamics in the unfolded state, the observation of a rather isotropic, random coil-like collapse of unfolded Csp[18] at low GdmCl concentrations suggests that such interactions might indeed be absent. In principle, conformational dynamics in denatured states of proteins can apparently occur on a very broad range of time scales and might be highly specific for every protein—even extremely slow dynamics cannot be excluded, such as those on the 100 s time scale inferred from single-molecule experiments on RNase H[72]—but their structural basis is often unclear. On the other hand, the nanosecond dynamics that are dominant in the unfolded state of Csp are most probably a universal characteristic of unfolded proteins, as suggested by comparison with the time scales of chain dynamics found in unstructured model peptides[7−9,49,57] and the observation of dynamics on a similar time scale for a series of other unfolded proteins[73] (Nettels, Hillger, Wuttke, and Schuler, unpublished observations). The corresponding process of elementary chain reconfiguration thus provides a reasonable value for the diffusion of a polypeptide chain on its conformational energy landscape, or the "speed limit" for protein folding reactions. The current "record holders" in terms of fast protein folding, which probably approach the "speed limit"[53] expected for a "downhill" process, are in the range of several hundred nanoseconds[54] to a few microseconds,[53,56,74] similar to the preexponential factor of 0.4 μs estimated from the reconfiguration time of unfolded Csp.[21]

While our previous experiments were done on terminally labeled Csp, an important question for protein folding is how the relative position of residues within the polypeptide sequence affects the time scale of intramolecular distance fluctuations between them. This issue of "external" versus "internal" loop formation has been addressed in a range of theoretical[75−80] and experimental work,[63,65,81] especially in polymer physics, and more recently also for unstructured polypeptides. In general, two effects would be expected to influence the position dependence of loop formation kinetics. First, the additional residues of the "tail" segment will contribute excluded volume in the vicinity of the residues probed, thus changing the underlying equilibrium distance distribution between them and reducing their probability of approaching each other. Second, there could be dynamic effects resulting from additional viscous drag of the tail segment or altered interactions within the chain.

In our experiments, we change the distance distribution between the probed residues both by moving the dyes closer within the chain and by concurrently increasing the tail segment length. However, as we can obtain the resulting change in the equilibrium distance distribution between the donor and acceptor from measurements of the transfer efficiency and the fluorescence lifetime decay in the unfolded subpopulation,[18] we can obtain direct information about the change in polypeptide dynamics, that is, the relative diffusion coefficient D between the two points in the chain. We observe a decrease in D with decreasing separation within the sequence (Figure 6c). D depends both on the change in viscous drag, which would be expected to increase with tail length, and on the details of the interactions within the chain, that is, between the backbone and side chains of the polypeptide. As previous experiments have indicated a rather uniform collapse of the chain,[18] suggesting a uniform distribution of interactions within the unfolded protein, the increase in viscous drag appears to dominate the change in D. It would of course be interesting to know whether there is a turnover of the position dependence of D for even shorter sequence separations, as expected from theory and as possibly suggested by the nonlinearity of the dependence of D on sequence separation in our data (Figure 6c), but shorter distances cannot be probed reliably with our current dye pair because of its large Förster radius.

A method that can be used for probing shorter distance dynamics is triplet state quenching, and it has previously been used to investigate the effect of tail segment length on loop formation in unstructured peptides.[63,65] Experiments using tryptophan triplet state quenching by cysteine indicated a very strong effect already from adding a single amino acid to the terminus, with not much change when the tail segment was lengthened further.[63] This result was interpreted in terms of the dominance of the first residue in shielding the quencher, which is reasonable in view of the fact that the cysteine side chain must essentially make van der Waals contact with tryptophan to quench its triplet state,[82] and especially considering the small size of the thiol group. In a different study, where the larger groups xanthone and napthylalanine were incorporated into peptides to investigate the formation of interior loops by triplet quenching, the contact rate was found to decrease continuously with tail length up to more than 20 residues.[65] While this result exhibits a qualitatively similar trend as we observe in unfolded Csp, a quantitative comparison to the intramolecular diffusion coefficients determined here is complicated by the lack of information on the interprobe distance distribution in these experiments.

Conclusions

The analysis of single-molecule photon statistics has become an increasingly valuable tool for our understanding of biomolecular dynamics on a wide range of time scales. For molecules freely diffusing in solution, the accessible time scales range from nanoseconds to the diffusion time through the confocal volume, typically in the range of several hundred microseconds. Using complete correlation functions from picoseconds to seconds, we showed that the dynamics of unstructured peptides labeled with a FRET pair can be analyzed down to the low nanosecond range and found no evidence for dynamics slower than in the tens of nanoseconds range for unfolded Csp. Upon moving one of the fluorophores from the terminus of Csp toward the center of the

sequence, we observed a substantial decrease of the intramolecular diffusion coefficient, presumably resulting from the viscous drag of the tail segment. The methodology used here should be applicable to a large number of questions, especially for processes with heterogeneous kinetics, in complex environments, or in cases where a synchronization of the ensemble by perturbation methods is difficult. Developments such as the gentle immobilization of proteins[72,83,84] or the use of ratios of correlation functions to eliminate the diffusive component[85,86] will help to extend the accessible time scales even further.

Acknowledgment. We thank Attila Szabo for many insightful and delectable discussions over the years. We thank Irina Gopich for advice on photon statistics and diffusive processes and for providing the algorithms to calculate correlation functions numerically. This work was supported by the Swiss National Science Foundation, the Human Frontier Science Program, the Swiss National Center of Competence in Research for Structural Biology, and the VolkswagenStiftung.

References and Notes

(1) Millett, I. S.; Doniach, S.; Plaxco, K. W. *Adv. Protein Chem.* **2002**, *62*, 241.
(2) Kohn, J. E.; Millett, I. S.; Jacob, J.; Zagrovic, B.; Dillon, T. M.; Cingel, N.; Dothager, R. S.; Seifert, S.; Thiyagarajan, P.; Sosnick, T. R.; Hasan, M. Z.; Pande, V. S.; Ruczinski, I.; Doniach, S.; Plaxco, K. W. *Proc. Natl. Acad. Sci. U.S.A.* **2004**, *101*, 12491.
(3) Vendruscolo, M. *Curr. Opin. Struct. Biol.* **2007**, *17*, 15.
(4) Mittag, T.; Forman-Kay, J. D. *Curr. Opin. Struct. Biol.* **2007**, *17*, 3.
(5) Shortle, D. R. *Curr. Opin. Struct. Biol.* **1996**, *6*, 24.
(6) Dyson, H. J.; Wright, P. E. *Chem. Rev.* **2004**, *104*, 3607.
(7) Bieri, O.; Wirz, J.; Hellrung, B.; Schutkowski, M.; Drewello, M.; Kiefhaber, T. *Proc. Natl. Acad. Sci. U.S.A.* **1999**, *96*, 9597.
(8) Lapidus, L. J.; Eaton, W. A.; Hofrichter, J. *Proc. Natl. Acad. Sci. U.S.A.* **2000**, *97*, 7220.
(9) Hudgins, R. R.; Huang, F.; Gramlich, G.; Nau, W. M. *J. Am. Chem. Soc.* **2002**, *124*, 556.
(10) Neuweiler, H.; Schulz, A.; Böhmer, M.; Enderlein, J.; Sauer, M. *J. Am. Chem. Soc.* **2003**, *125*, 5324.
(11) Jia, Y. W.; Talaga, D. S.; Lau, W. L.; Lu, H. S. M.; DeGrado, W. F.; Hochstrasser, R. M. *Chem. Phys.* **1999**, *247*, 69.
(12) Haran, G. *J. Phy.: Condens. Matter* **2003**, *15*, R1291.
(13) Schuler, B. *ChemPhysChem* **2005**, *6*, 1206.
(14) Michalet, X.; Weiss, S.; Jager, M. *Chem. Rev.* **2006**, *106*, 1785.
(15) Schuler, B.; Eaton, W. A. *Curr. Opin. Struct. Biol.* **2008**, *18*, 16.
(16) Ha, T.; Enderle, T.; Ogletree, D. F.; Chemla, D. S.; Selvin, P. R.; Weiss, S. *Proc. Natl. Acad. Sci. U.S.A.* **1996**, *93*, 6264.
(17) Schuler, B.; Lipman, E. A.; Steinbach, P. J.; Kumke, M.; Eaton, W. A. *Proc. Natl. Acad. Sci. U.S.A.* **2005**, *102*, 2754.
(18) Hoffmann, A.; Kane, A.; Nettels, D.; Hertzog, D. E.; Baumgärtel, P.; Lengefeld, J.; Reichardt, G.; Horsley, D. A.; Seckler, R.; Bakajin, O.; Schuler, B. *Proc. Natl. Acad. Sci. U.S.A.* **2007**, *104*, 105.
(19) Laurence, T. A.; Kong, X. X.; Jäger, M.; Weiss, S. *Proc. Natl. Acad. Sci. U.S.A.* **2005**, *102*, 17348.
(20) Neuweiler, H.; Doose, S.; Sauer, M. *Proc. Natl. Acad. Sci. U.S.A.* **2005**, *102*, 16650.
(21) Nettels, D.; Gopich, I. V.; Hoffmann, A.; Schuler, B. *Proc. Natl. Acad. Sci. U.S.A.* **2007**, *104*, 2655.
(22) Perl, D.; Welker, C.; Schindler, T.; Schröder, K.; Marahiel, M. A.; Jaenicke, R.; Schmid, F. X. *Nat. Struct. Biol.* **1998**, *5*, 229.
(23) Wassenberg, D.; Welker, C.; Jaenicke, R. *J. Mol. Biol.* **1999**, *289*, 187.
(24) Schuler, B.; Lipman, E. A.; Eaton, W. A. *Nature* **2002**, *419*, 743.
(25) Schuler, B.; Kremer, W.; Kalbitzer, H. R.; Jaenicke, R. *Biochemistry* **2002**, *41*, 11670.
(26) Lipman, E. A.; Schuler, B.; Bakajin, O.; Eaton, W. A. *Science* **2003**, *301*, 1233.
(27) Kurtsiefer, C.; Zarda, P.; Mayer, S.; Weinfurter, H. *J. Mod. Opt.* **2001**, *48*, 2039.
(28) Berglund, A. J.; Doherty, A. C.; Mabuchi, H. *Phys. Rev. Lett.* **2002**, *89*, 068101.
(29) Wang, Z. S.; Makarov, D. E. *J. Phys. Chem. B* **2003**, *107*, 5617.
(30) Rigler, R.; Elson, E. S. *Flourescence Correlation Spectroscopy: Theory and Applications*; Springer: Berlin, Germany, 2001.
(31) Hübner, C. G.; Zumofen, G.; Renn, A.; Herrmann, A.; Müllen, K.; Basché, T. *Phys. Rev. Lett.* **2003**, *91*.
(32) De Schryver, F. C.; Vosch, T.; Cotlet, M.; Van, der Auweraer, M.; Müllen, K.; Hofkens, J. *Acc. Chem. Res.* **2005**, *38*, 514.
(33) Bradforth, S. E.; Jinenez, R.; Vanmourik, F.; Vangrondelle, R.; Fleming, G. R. *J. Phys. Chem.* **1995**, *99*, 16179.
(34) Kapusta, P.; Erdmann, R.; Ortmann, U.; Wahl, M. *J. Fluoresc.* **2003**, *13*, 179.
(35) Lakowicz, J. R. *Principles of Fluorescence Spectroscopy*, 2nd ed.; Kluwer Academic/Plenum Publishers: New York, 1999.
(36) Lipari, G.; Szabo, A. *Biophys. J.* **1980**, *30*, 489.
(37) Hanbury Brown, R.; Twiss, R. Q. *Nature* **1956**, *177*, 27.
(38) Ehrenberg, M.; Rigler, R. *Chem. Phys.* **1974**, *4*, 390.
(39) Fleury, L.; Segura, J. M.; Zumofen, G.; Hecht, B.; Wild, U. P. *Phys. Rev. Lett.* **2000**, *84*, 1148.
(40) Tinnefeld, P.; Müller, C.; Sauer, M. *Chem. Phys. Lett.* **2001**, *345*, 252.
(41) Weston, K. D.; Dyck, M.; Tinnefeld, P.; Müller, C.; Herten, D. P.; Sauer, M. *Anal. Chem.* **2002**, *74*, 5342.
(42) Hofkens, J.; Cotlet, M.; Vosch, T.; Tinnefeld, P.; Weston, K. D.; Ego, C.; Grimsdale, A.; Mullen, K.; Beljonne, D.; Bredas, J. L.; Jordens, S.; Schweitzer, G.; Sauer, M.; De Schryver, F. *Proc. Natl. Acad. Sci. U.S.A.* **2003**, *100*, 13146.
(43) Nettels, D.; Schuler, B. *IEEE J. Sel. Top. Quant. Electron.* **2007**, *13*, 990.
(44) Felekyan, S.; Kühnemut, R.; Kudryavtsev, V.; Sandhagen, C.; Becker, W.; Seidel, C. A. M. *Rev. Sci. Instrum.* **2005**, *76*, 083104.
(45) Wahl, M.; Rahn, H. J.; Gregor, I.; Erdmann, R.; Enderlein, J. *Rev. Sci. Instrum.* **2007**, *78*, 033106.
(46) Gopich, I. V.; Szabo, A. *J. Chem. Phys.* **2006**, *124*, 154712.
(47) Mets, Ü. Antibunching and Rotational Diffusion in FCS. In *Fluorescence Correlation Spectroscopy*; Elson, E. S., Rigler, R., Eds.; Springer-Verlag: Berlin, Germany, 2001.
(48) Haas, E.; Katchalskikatzir, E.; Steinberg, I. Z. *Biopolymers* **1978**, *17*, 11.
(49) Möglich, A.; Joder, K.; Kiefhaber, T. *Proc. Natl. Acad. Sci. U.S.A.* **2006**, *103*, 12394.
(50) Eggeling, C.; Kask, P.; Winkler, D.; Jäger, S. *Biophys. J.* **2005**, *89*, 605.
(51) Bryngelson, J. D.; Onuchic, J. N.; Socci, N. D.; Wolynes, P. G. *Proteins* **1995**, *21*, 167.
(52) Socci, N. D.; Onuchic, J. N.; Wolynes, P. G. *J. Chem. Phys.* **1996**, *104*, 5860.
(53) Kubelka, J.; Hofrichter, J.; Eaton, W. A. *Curr. Opin. Struct. Biol.* **2004**, *14*, 76.
(54) Kubelka, J.; Chiu, T. K.; Davies, D. R.; Eaton, W. A.; Hofrichter, J. *J. Mol. Biol.* **2006**, *359*, 546.
(55) Hagen, S. J.; Hofrichter, J.; Szabo, A.; Eaton, W. A. *Proc. Natl. Acad. Sci. U.S.A.* **1996**, *93*, 11615.
(56) Yang, W. Y.; Gruebele, M. *Nature* **2003**, *423*, 193.
(57) Lapidus, L. J.; Steinbach, P. J.; Eaton, W. A.; Szabo, A.; Hofrichter, J. *J. Phys. Chem. B* **2002**, *106*, 11628.
(58) Roder, H.; Shastry, M. R. *Curr. Opin. Struct. Biol.* **1999**, *9*, 620.
(59) Bilsel, O.; Matthews, C. R. *Curr. Opin. Struct. Biol.* **2006**, *16*, 86.
(60) Schwille, P. Cross-Correlation Analysis in FCS. In *Fluorescence Correlation Spectroscopy*; Elson, E. S., Rigler, R., Eds.; Springer-Verlag: Berlin, Germany, 2001.
(61) Widengren, J.; Mets, Ü.; Rigler, R. *J. Phys. Chem.* **1995**, *99*, 13368.
(62) Best, R.; Merchant, K.; Gopich, I. V.; Schuler, B.; Bax, A.; Eaton, W. A. *Proc. Natl. Acad. Sci. U.S.A.* **2007**, *104*, 18964.
(63) Buscaglia, M.; Lapidus, L. J.; Eaton, W. A.; Hofrichter, J. *Biophys. J.* **2006**, *91*, 276.
(64) Krieger, F.; Fierz, B.; Bieri, O.; Drewello, M.; Kiefhaber, T. *J. Mol. Biol.* **2003**, *332*, 265.
(65) Fierz, B.; Kiefhaber, T. *J. Am. Chem. Soc.* **2007**, *129*, 672.
(66) Deniz, A. A.; Laurence, T. A.; Beligere, G. S.; Dahan, M.; Martin, A. B.; Chemla, D. S.; Dawson, P. E.; Schultz, P. G.; Weiss, S. *Proc. Natl. Acad. Sci. U.S.A.* **2000**, *97*, 5179.
(67) Kramers, H. A. *Physica* **1940**, *7*, 284.
(68) Klimov, D. K.; Thirumalai, D. *Phys. Rev. Lett.* **1997**, *79*, 317.
(69) Reference deleted in proof.
(70) Jacob, M.; Holtermann, G.; Perl, D.; Reinstein, J.; Schindler, T.; Geeves, M. A.; Schmid, F. X. *Biochemistry* **1999**, *38*, 2882.
(71) Magg, C.; Kubelka, J.; Holtermann, G.; Haas, E.; Schmid, F. X. *J. Mol. Biol.* **2006**, *360*, 1067.
(72) Kuzmenkina, E. V.; Heyes, C. D.; Nienhaus, G. U. *Proc. Natl. Acad. Sci. U.S.A.* **2005**, *102*, 15471.
(73) Sadqi, M.; Lapidus, L. J.; Munoz, V. *Proc. Natl. Acad. Sci. U.S.A.* **2003**, *100*, 12117.
(74) Naganathan, A. N.; Doshi, U.; Munoz, V. *J. Am. Chem. Soc.* **2007**, *129*, 5673.
(75) Friedman, B.; Oshaughnessy, B. *Macromolecules* **1993**, *26*, 4888.
(76) Chan, H. S.; Dill, K. A. *J. Chem. Phys.* **1989**, *90*, 492.
(77) Sheng, Y. J.; Hsu, P. H.; Chen, J. Z. Y.; Tsao, H. K. *Macromolecules* **2004**, *37*, 9257.

(78) Zhou, H. X. *Biochemistry* **2004**, *43*, 2141.
(79) Pastor, R. W.; Zwanzig, R.; Szabo, A. *J. Chem. Phys.* **1996**, *105*, 3878.
(80) Wang, Z. S.; Makarov, D. E. *J. Chem. Phys.* **2002**, *117*, 4591.
(81) Doucet, D.; Roitberg, A.; Hagen, S. J. *Biophys. J.* **2007**, *92*, 2281.
(82) Lapidus, L. J.; Eaton, W. A.; Hofrichter, J. *Phys. Rev. Lett.* **2001**, *8725*, 8101.
(83) Rhoades, E.; Gussakovsky, E.; Haran, G. *Proc. Natl. Acad. Sci. U.S.A.* **2003**, *100*, 3197.
(84) Rhoades, E.; Cohen, M.; Schuler, B.; Haran, G. *J. Am. Chem. Soc.* **2004**, *126*, 14686.
(85) Li, G.; Levitus, M.; Bustamante, C.; Widom, J. *Nat. Struct. Mol. Biol.* **2005**, *12*, 46.
(86) Torres, T.; Levitus, M. *J. Phys. Chem. B* **2007**, *111*, 7392.

THE JOURNAL OF PHYSICAL CHEMISTRY B

Addition/Correction

pubs.acs.org/JPCB

Correction to "Unfolded Protein and Peptide Dynamics Investigated with Single-Molecule FRET and Correlation Spectroscopy from Picoseconds to Seconds"

Daniel Nettels, Armin Hoffmann, and Benjamin Schuler*

J. Phys. Chem. B **2008**, *112* (19), 6137−6146. DOI: 10.1021/jp076971j

In this work, we reported, among other aspects, results on the chain dynamics in the unfolded state of the small cold shock protein from *Thermotoga maritima* (Csp), determined using nanosecond fluorescence correlation spectroscopy (FCS) in combination with Förster resonance energy transfer (FRET). Recent experiments in our laboratory have now shown that some of the correlation times given in Figure 6b are not only due to fluctuations in the FRET rate but contain a contribution from static quenching of the donor and/or acceptor fluorophores by the tryptophan residues within the chain.[1] As a result, for some of the variants, the conversion of the reported decay times of the intensity correlation functions, τ_{CD}, to decay times of the intramolecular *distance* correlation time, τ_r, and to intramolecular diffusion coefficients, D (Figure 6c), are affected significantly by this additional quenching component. Recent measurements on Csp without tryptophan residues show that τ_{CD} and τ_r increase with increasing sequence separation,[1] as expected for a Rouse chain,[2] but additional effects from internal friction have to be taken into account to explain the behavior quantitatively.[1] None of the other results are affected. Note also that fluorophores positioned at the chain termini of Csp (position 2 and 67) are not influenced by tryptophan quenching, and the values of τ_r reported for this variant are unaffected, both here and in earlier work.[3] In that case, and in all other published work where we use nanosecond FCS, the absence of quenching by tryptophan was verified in experiments employing, e.g., direct excitation of the acceptor and samples labeled only with donor dye.

REFERENCES

(1) Soranno, A.; et al. Quantifying internal friction in unfolded and intrinsically disordered proteins with single molecule spectroscopy. *Proc. Natl. Acad. Sci. U.S.A.* early edition, www.pnas.org/cgi/doi/10.1073/pnas.1117368109 (**2012**).

(2) Makarov, D. E. Spatiotemporal correlations in denatured proteins: The dependence of fluorescence resonance energy transfer (FRET)-derived protein reconfiguration times on the location of the FRET probes. *J. Chem. Phys.* **2010**, *132*, 035104.

(3) Nettels, D.; Gopich, I. V.; Hoffmann, A.; Schuler, B. Ultrafast dynamics of protein collapse from single-molecule photon statistics. *Proc. Natl. Acad. Sci. U.S.A.* **2007**, *104*, 2655−2660.

Published: May 3, 2012